Aberrant Buildup of All-*Trans*-Retinal Dimer, a Nonpyridinium Bisretinoid Lipofuscin Fluorophore, Contributes to the Degeneration of the Retinal Pigment Epithelium

Junli Zhao,[1,2] Yi Liao,[1] Jingmeng Chen,[1] Xinran Dong,[3] Zhan Gao,[1] Houjian Zhang,[1] Xiaodan Wu,[4] Zuguo Liu,[1] and Yalin Wu[1]

[1]Fujian Provincial Key Laboratory of Ophthalmology and Visual Science, Eye Institute of Xiamen University, College of Medicine, Xiamen University, Xiamen, China
[2]College of Pharmaceutical Sciences, Zhejiang University, Hangzhou, China
[3]Department of Ophthalmology, Guangdong Academy of Medical Science, Guangdong General Hospital, Guangzhou, China
[4]Center of Analysis and Measurement, Zhejiang University, Hangzhou, China

Correspondence: Yalin Wu, Fujian Provincial Key Laboratory of Ophthalmology and Visual Science, Eye Institute of Xiamen University, College of Medicine, Xiamen University, Xiang'an South Road, Xiamen 361102, China;
yalinw@xmu.edu.cn.

Submitted: September 12, 2016
Accepted: January 11, 2017

Citation: Zhao J, Liao Y, Chen J, et al. Aberrant buildup of all-*trans*-retinal dimer, a nonpyridinium bisretinoid lipofuscin fluorophore, contributes to the degeneration of the retinal pigment epithelium. *Invest Ophthalmol Vis Sci*. 2017;58:1063–1075. DOI: 10.1167/iovs.16-20734

Purpose. Nondegradable fluorophores that accumulate as deleterious lipofuscin of RPE are involved in pathological mechanisms leading to the degeneration of RPE in AMD. A2E, a major component of RPE lipofuscin, could cause damage to RPE cells. Nevertheless, all-*trans*-retinal dimer (atRAL dimer) was found to be much more abundant than that of A2E in eyes of $Abca4^{-/-}Rdh8^{-/-}$ double-knockout (DKO) mice, a rodent model showing the typical characteristics of retinopathies in AMD patients. Our aim was to elucidate the effect and mechanism of atRAL dimer–induced RPE degeneration.

Methods. Eyes harvested from C57BL/6J wild-type (WT) and $Abca4^{-/-}Rdh8^{-/-}$ DKO mice were examined by HPLC. Cellular uptake, subcellular localization, 5-bromo-2-deoxyuridine (BrdU), Cdc25C, DNA strand breaks, mitochondrial membrane potential ($\Delta\Psi m$), and cytochrome *c* were analyzed by fluorescence microscopy. Cellular toxicity was assayed by lactate dehydrogenase (LDH) assay and dead cell staining. Apoptosis and cell-cycle stages were detected by flow cytometry. Furthermore, in vitro and in vivo expression of proteins associated with cell cycle and apoptosis was measured by immunoblot assays.

Results. All-*trans*-retinal dimer clearly could damage RPE cell membrane and inhibit the proliferation of RPE cells as well as induce DNA damage and cell-cycle arrest at the G2/M phase via activating the ATM/ATR-Chk2-p53 signaling pathway. Moreover, this di-retinal adduct triggered mitochondrion-associated apoptosis in RPE cells. Evidence from the cell-based experiments was also corroborated by a remarkable abnormality in expression of proteins associated with cell cycle (Cyclin B1 and Cdc2) and apoptosis (p53, Bcl-2 and Bax) in the RPE of $Abca4^{-/-}Rdh8^{-/-}$ DKO mice.

Conclusions. These findings suggest that atRAL dimer that accumulates beyond a critical level, facilitates age-dependent RPE degeneration.

Keywords: all-*trans*-retinal dimer, bisretinoid lipofuscin, retinal pigment epithelium, cell cycle, proliferation inhibition, mitochondrial dysfunction

Age-related macular degeneration (AMD) is a retinal degenerative disease that is a major cause of irreversible vision loss in individuals older than 50 years in many developed countries, especially in the United States.[1–3] In the latest estimates undertaken by the World Health Organization, AMD affects more than 30 million people, and incurs legal blindness in more than 500,000 patients with AMD annually. The etiology of AMD is implicated with RPE and photoreceptor degeneration.[4] Gradual accumulation of autofluorescent lipofuscin in the lysosomal storage bodies of the RPE is a hallmark of aging in vertebrates.[5] High levels of RPE lipofuscin have been considered to be associated with degeneration of the RPE[6,7] and concomitant disturbance in the daily phagocytosis of shed photoreceptor outer segments by RPE cells, a critical process for the maintenance of the retina.[8] Although excess deposition of lipofuscin pigment granules in the RPE contributes to increased morbidity of AMD, the mechanism underlying RPE lipofuscin-induced retinal degeneration is not fully understood as yet. An inadvertent consequence of retinal metabolism necessary for regeneration of visual chromophore 11-*cis*-retinal is the formation of retinal-derived compounds that undergo synthesis in photoreceptor outer segments of neural retina and are secondarily deposited in the RPE as predominant hydrophobic components of toxic lipofuscin.[9,10] Several lipofuscin fluorophores have been structurally identified in vertebrate RPE, including A2E (Fig. 1A),[11] isoA2E,[12] iisoA2E,[13] all-*trans*-retinal dimer (atRAL dimer) (Fig. 1B),[14] A2-DHP-PE,[15] pdA2E,[16] and isopdA2E.[17] In all of these pigments, the most intense and

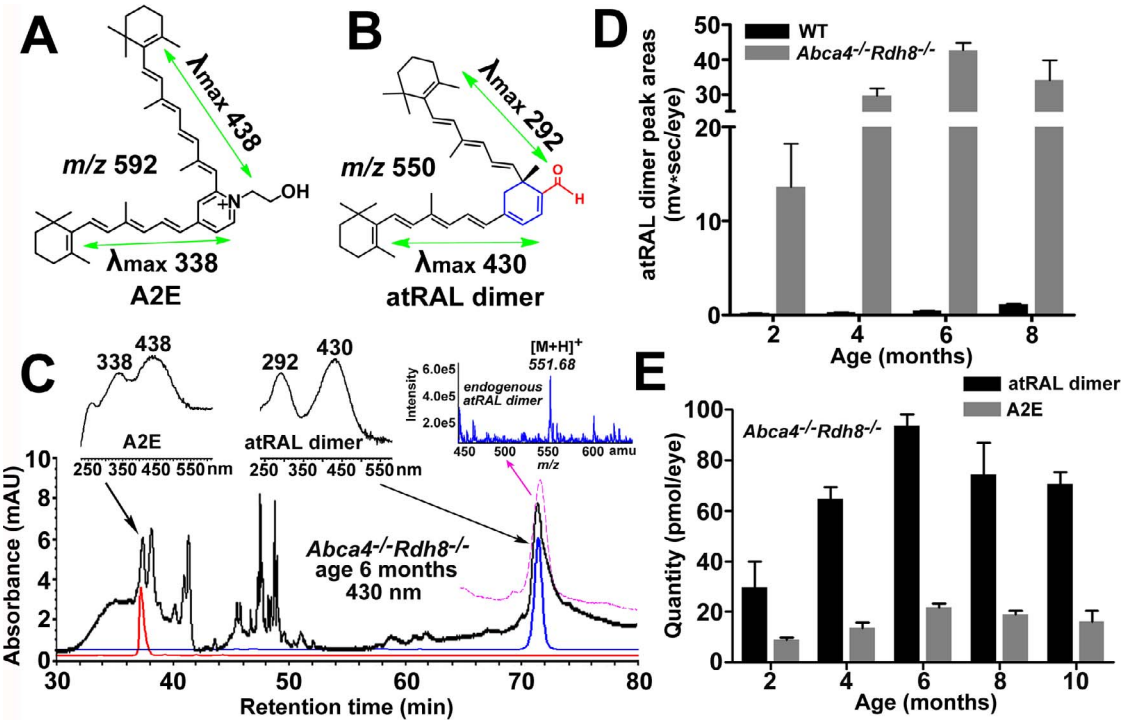

Figure 1. Measurement of atRAL dimer and A2E in *Abca4*$^{-/-}$*Rdh8*$^{-/-}$ DKO and WT mice. (**A**, **B**) A2E and atRAL dimer: structures, UV-visible absorbance maxima (λmax), mass-to-charge ratio (*m/z*), and electronic transition assignments (↔). (**C**) A representative reverse-phase HPLC chromatogram of a hydrophobic extract of six eyes harvested from 6-month-old *Abca4*$^{-/-}$*Rdh8*$^{-/-}$ DKO mice was overlaid with that of synthesized A2E (*red*) and atRAL dimer (*blue*) as well as endogenous atRAL dimer (*dotted pink*) in 10 eyes from *Abca4*$^{-/-}$*Rdh8*$^{-/-}$ DKO mice at 6 to 10 months of age. *Top insets*: UV-visible absorbance spectra of A2E and atRAL dimer peak fractions isolated from eyes of 6-month-old *Abca4*$^{-/-}$*Rdh8*$^{-/-}$ DKO mice. *Inset on the right*: ESI-MS spectrum of atRAL dimer from 10 eyes of *Abca4*$^{-/-}$*Rdh8*$^{-/-}$ DKO mice at 6 to 10 months of age. All-*trans*-retinal dimer has a mass of 550.86. (**D**) All-*trans*-retinal dimer in C57BL/6J WT and *Abca4*$^{-/-}$*Rdh8*$^{-/-}$ DKO mice at ages 2, 4, 6, and 8 months was measured using HPLC. Integrated peak areas (mV•s) were calculated using Empower version 3 software, and presented as mean ± SEM of three to four samples. (**E**) All-*trans*-retinal dimer and A2E in mutant (*Abca4*$^{-/-}$*Rdh8*$^{-/-}$) mice at 2, 4, 6, 8, and 10 months of age were quantified by reverse-phase HPLC. Integrated peak areas (mV•s) were converted into picomolar quantities by using standard calibration curves (Supplementary Fig. S1). Data were expressed as mean ± SEM of three samples.

extensive studies are directed to A2E due to its abundance and typical age-dependent accumulation in humans,[18] and C57BL/6J and BALB/cByJ wild-type (WT) mice.[15]

Previous studies have indicated that *Abca4*$^{-/-}$*Rdh8*$^{-/-}$ double-knockout (DKO) mice reproduce the main features of human AMD in a rodent model.[19–21] Palczewski and coworkers carried out HPLC quantification of atRAL dimer in eyes of *Abca4*$^{-/-}$*Rdh8*$^{-/-}$ DKO mice versus WT mice at 3 and 6 months of age, and demonstrated that the amount of atRAL dimer in *Abca4*$^{-/-}$*Rdh8*$^{-/-}$ DKO mice increased significantly and age-dependently.[19] Additionally, histological evidence revealed that the dramatic retinal degeneration in *Abca4*$^{-/-}$*Rdh8*$^{-/-}$ DKO mice initiated at the age of 1.0 to 1.5 months, and rapidly worsened with age ranging from 3.0 to 6.0 months.[19] Based on these phenomena, this age-dependent phenotype in the retina of *Abca4*$^{-/-}$*Rdh8*$^{-/-}$ DKO mice is possibly associated with the exacerbated accumulation of atRAL dimer in the RPE. Accordingly, the objective of this study was to elucidate the potential role of atRAL dimer in the occurrence and development of RPE degeneration.

Materials and Methods

Animals

C57BL/6J WT mice were purchased from Shanghai SLAC Laboratory Animal Co. Ltd. (Shanghai, China), and C57BL/6N mice were purchased from the Model Animal Research Center of Nanjing University (Nanjing, China). Genotyping of mice and sequencing of mutations were carried out according to a previous report.[22] *Abca4*$^{-/-}$*Rdh8*$^{-/-}$ DKO mice were kindly donated by the Krzysztof Palczewski Laboratory (Case Western Reserve University, Cleveland, OH, USA). All these mice were raised under 12 hour on/off cyclic lighting with an in-cage illuminance of approximately 180 to 230 lux in the Laboratory Animal Center of Xiamen University. Experiments with animals were performed in accordance with protocols approved by the Institutional Animal Care and Use Committee of Xiamen University Medical College, and adherent to the ARVO Statement for the Use of Animals in Ophthalmic and Vision Research.

Eye Extracts and HPLC Analysis

Murine eyes (4–13 eyes/sample) were homogenized in a vol/vol solution of PBS/deuterium-depleted water and 50% methanolic chloroform, as previously reported.[13] Each extract was examined by reverse-phase HPLC using an Alliance System (Waters Corp., Milford, MA, USA) equipped with a 2695 separation module, a 2998 photodiode array detector, and a 2475 multichannel (λ) fluorescence detector. For compound elution, an analytical scale Atlantis (Milford, MA, USA) dC18 (3 μm, 4.6 × 150 mm) column was used with a gradient mobile phase consisting of acetonitrile and water in the presence of 0.1% trifluoroacetic acid: 75% to 90% acetonitrile (0–30 minutes), 90% to 100% acetonitrile (30–40 minutes), and 100% acetonitrile (40–100 minutes), with a flow rate of 0.5 mL/min. Photodiode array detection was monitored at 430 nm.

Peak area (μV•s; 1 mV•s = 1000 μV•s) was integrated using Empower version 3 software (Waters Corp.). Molar quantity per eye was calculated using calibration curves constructed from known concentrations and integrated HPLC peak areas of synthesized standards (Supplementary Fig. S1). Compounds in the extract of 10 eyes from *Abca4*$^{-/-}$*Rdh8*$^{-/-}$ DKO mice at 6 to 10 months of age were ionized by electrospray ionization (ESI) operated in a positive ion mode and analyzed by using an API 3200 Q-Trap LC/MS/MS instrument supplied by Applied Biosystems (Foster City, CA, USA). The same dC18 column and mobile phase was used as described above for HPLC.

Synthesis

All-*trans*-retinal dimer was synthesized in vitro as described previously,[14] with minor modifications. Briefly, a chemical reaction mixture of atRAL (50 mg, 0.176 mM) and NaH (4.23 mg, 0.176 mM) in 3 mL anhydrous tetrahydrofuran (THF) was stirred for 3 hours at room temperature in the dark, and terminated by slow addition of a saturated ammonium chloride (NH_4Cl) solution. The resulting mixture was extracted with diethyl ether (Et_2O), and dried using saturated sodium chloride and anhydrous sodium sulphate. After the solvents were concentrated to dry with a rotary evaporator, the silica gel column chromatography with an eluent of hexane/methylene chloride (4:1, vol/vol) afforded approximately 12 mg of atRAL dimer in pure form. The A2E was synthesized as published.[12] The identity and purity of synthesized A2E and atRAL dimer were corroborated by proton nuclear magnetic resonance spectroscopy, UV-visible absorbance, and reverse-phase HPLC with monitoring at 430 nm (Supplementary Figs. S2–S4).

Cell Culture and Treatments

A human RPE cell line (ARPE-19), purchased from FuDan IBS Cell Center (Shanghai, China), was grown in Dulbecco's modified Eagle medium (DMEM) (HyClone, Logan, UT, USA) supplemented with 10% heat-inactivated fetal bovine serum (HyClone), penicillin (100 units/mL), and streptomycin (100 μg/mL) in a humidified incubator with 5% CO_2 at 37°C. A stock solution of atRAL dimer (40 mM) was prepared with dimethyl sulfoxide (DMSO), and ARPE-19 cells were incubated with serial dilutions of atRAL dimer (0, 2.5, 5, 10, 20, 40, and 80 μM) for 1 to 3 days.

Cellular Uptake and Subcellular Localization

ARPE-19 cells were incubated with atRAL dimer at indicated concentrations for 3 days in 24-well cell culture plates. Uptake of atRAL dimer by cells was detected and imaged using a laser scanning confocal microscope (LSM510 Meta; Carl Zeiss, Heidelberg, Germany) with an argon-krypton laser (atRAL dimer, Ex 488 nm and Em 530 nm; 4′,6-diamidino-2-phenylindole [DAPI], Ex 405 nm and Em 426–489 nm). To determine where atRAL dimer localized within RPE cells, cells grown in 24-well cell culture plates were simultaneously incubated with atRAL dimer (20 μM) and LysoTracker Red DND-99 (50 nM; Molecular Probes, Invitrogen, Waltham, MA, USA) in culture medium for 45 minutes. Cells were washed in fresh and prewarmed PBS, and fixed with 4% paraformaldehyde for 15 minutes at 4°C in the dark. After rinsing the cells with PBS, photographs were taken by the confocal microscope.

Cellular Toxicity Tests

Cellular toxicity was assessed by lactate dehydrogenase (LDH) assay and dead cell staining. Cells seeded in 96-well plates (6×10^3 cells/well) were incubated with atRAL dimer (0–80 μM). Lactate dehydrogenase assay was performed by using an LDH Cytotoxicity Assay Kit (Beyotime, Haimen, China). Cytoplasmic LDH was measured in culture medium after 2- and 5-day incubations of atRAL dimer with cells in fresh serum-free medium by using the microplate reader at 490 nm absorbance. After 3-day treatment, the nuclei of membrane-permeabilized cells were also labeled with 5 nM Dead Red (Molecular Probes, Invitrogen), and nuclei of all cells were stained by DAPI (1:1000 dilution; Beyotime).

Apoptosis Detection by Flow Cytometry

Differentiation between apoptotic versus necrotic types of cell death was studied by Annexin V and propidium iodide (PI) staining using the apoptosis detection kit (MultiSciences, Hangzhou, China). Briefly, after ARPE-19 cells were treated with atRAL dimer (0, 20, 40, and 80 μM) for 3 days, cells were harvested, washed in cold PBS, and then pelleted. Cells were resuspended in 500 μL binding buffer, and stained with 5 μL Annexin V-FITC (fluorescein isothiocyanate) and 10 μL PI in the dark for 5 minutes at room temperature, followed by flow cytometry analysis using a Cytomics FC500 flow cytometer (Beckman Coulter, Brea, CA, USA).

Single-Cell Gel Electrophoresis Assay

DNA strand breaks were probed using alkaline single-cell gel electrophoresis (comet assay). To prevent additional DNA damage, all processes were conducted under dim red light. Three days after exposure to atRAL dimer (0, 20, 40, and 80 μM), ARPE-19 cells were harvested, embedded in 0.5% agarose gel at a density of 1×10^6 cells/mL, and spread onto the fully frosted slides. Slides were immersed in ice-cold lysis solution at pH 10 and kept at 4°C for 3 hours; the lysis solution consisted of 2.5 M NaCl, 100 mM Na_2 EDTA, 10 mM Trizma base, 1% Triton X-100, and 10% DMSO. Then cellular DNA was allowed to unwind in the electrophoresis buffer, including 300 mM NaOH and 1 mM Na_2EDTA (pH $>$ 13) for 20 minutes, and electrophoresed for 20 minutes at a constant voltage of 25 V and 300 mA at 4°C. Next, the slides were neutralized with 0.4 M Tris-HCl (pH 7.5), dehydrated in ice-cold ethanol, and left to air dry. Samples were stained with 20 μg/mL ethidium bromide (EB) and then examined under a fluorescence inverted microscope (Axio Observer A1; Zeiss, Heidelberg, Germany). Fifty to 100 randomly selected cells per treatment were scored from three independent experiments and measured for the length of DNA comet tails.

Measurement of Mitochondrial Membrane Potential

Determination of the mitochondrial inner transmembrane potential ($\Delta\Psi m$) was carried out by a mitochondrial membrane potential assay kit with JC-1 (Beyotime). Briefly, after treating ARPE-19 cells with atRAL dimer (0, 20, 40, and 80 μM) for 3 days, 10^5 cells were harvested, resuspended in 500 μL DMEM medium, and stained with 500 μL JC-1 at 37°C for 20 minutes. After being washed using ice-cold staining buffer twice, cells were finally suspended in 500 μL staining buffer, and analyzed by the flow cytometer. Changes in MMP also were evaluated in situ by an inverted fluorescence microscope (BX61W1-FV1000; Olympus, Tokyo, Japan). For imaging of JC-1 monomers, the wavelengths were set at 490 nm for excitation and 530 nm for emission, and for JC-1 aggregates, the wavelengths were set at 525 nm and 590 nm for excitation and emission, respectively.

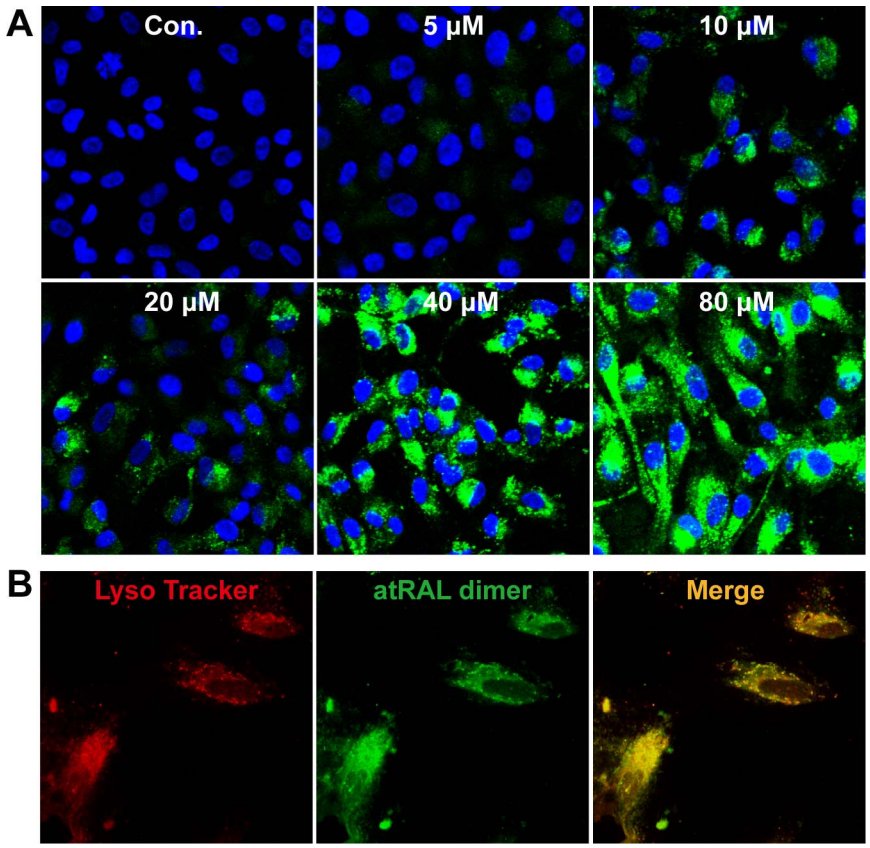

Figure 2. Detection of internalization and subcellular localization of atRAL dimer by confocal laser scanning fluorescence microscopy. (**A**) Retinal pigment epithelial cells were untreated or incubated with atRAL dimer (5, 10, 20, 40, and 80 μM) for 3 days. Then cells were fixed, and nuclei were stained with DAPI (*blue*). Internalized atRAL dimer granules exhibit *green autofluorescence* at excitation/emission of 488/505 to 550 nm, and perinuclear distribution of this adduct is evident. All-*trans*-retinal dimer granules that *fluoresce green* are augmented with increasing of atRAL dimer concentrations. *Scale bars*: 20 μm. (**B**) Colocalization of atRAL dimer with LysoTracker Red (Molecular Probes, Invitrogen). Microscopic autofluorescence signals at the *left* and in the *middle* are superimposed on the *right*; particles that colocalize in the *left* and *middle* appear *yellowish orange* on the *right* when *green* is combined with *red*.

Detection of Cell-Cycle Stages

Human RPE cells (ARPE-19) were treated with atRAL dimer (0, 20, 40, and 80 μM) for 3 days before testing the distribution of cell-cycle stages. Control and treated cells were collected into polypropylene tubes and pelleted at 2000 rpm for 5 minutes. Cells were then washed with precooling PBS twice and fixed with chilled 70% ethanol overnight at 4°C. Fixed cells were washed with PBS, and incubated in 0.5 mL PBS containing 50 μg RNase A, 25 μg PI, and 0.2% Triton X-100 at 4°C for 30 minutes in the dark. The DNA content was determined by the flow cytometer, and the percentage of cells at G0/G1, S, and G2/M phases was calculated using the MultiCycle software (Beckman Coulter).

Immunofluorescence Staining of Cytochrome *c*

Human RPE cells (ARPE-19) grown on glass cover slips were treated with atRAL dimer (0, 20, 40, and 80 μM) for 3 days, and subsequently incubated with 1 μM MitoTracker Red CM-H_2Xros at 37°C for 45 minutes. Cells were fixed with 4% paraformaldehyde at 4°C for 15 minutes, permeabilized with 0.5% Triton X-100 for 20 minutes, and then blocked with immunol staining blocking buffer (Beyotime) for 40 minutes. Afterward, cells were exposed to a monoclonal anti–Cytochrome *c* antibody (1:200 dilution; Cell Signaling Technology, Danvers, MA, USA) overnight at 4°C, followed by incubation with FITC-labeled Donkey anti-Rabbit secondary antibody (1:100 dilution; Jackson ImmunoResearch, West Grove, PA, USA) for 2 hours at room temperature. After extensive washes with 20 mM Tris-HCl (pH = 7.5), 137 mM NaCl, 0.1% Tween-20 (TTBS) and mounting by glycerol, these slides were examined by the confocal microscope.

Immunofluorescence Staining of Cdc25C

Human RPE cells (ARPE-19) seeded in 96-well culture plates were incubated with 0, 20, 40, and 80 μM atRAL dimer for 2 days. Cells were fixed with 4% paraformaldehyde for 20 minutes, and permeabilized with 0.5% Triton X-100 for 20 minutes. Human RPE cells (ARPE-19) that underwent pretreatment were incubated with immunol staining blocking buffer to block nonspecific staining for 30 minutes, followed by incubation with anti-Cdc25C antibody (1:200; Cell Signaling Technology) at 4°C overnight. After three washes with PBS, the resulting cells were incubated with Alexa Fluor 594-conjugated AffiniPure Donkey Anti-Rabbit IgG (H+L) for 2 hours at 37°C, counterstained with DAPI, and then analyzed with the fluorescence microscope.

Staining With 5-Bromo-2-Deoxyuridine

For 5-bromo-2-deoxyuridine (BrdU) (Sigma-Aldrich Corp., St. Louis, MO, USA) staining, 30 μM BrdU was added to the culture for the final 24 hours before fixation of ARPE-19 cells. Fixed cells were permeabilized with 1% Triton X-100, and denatured

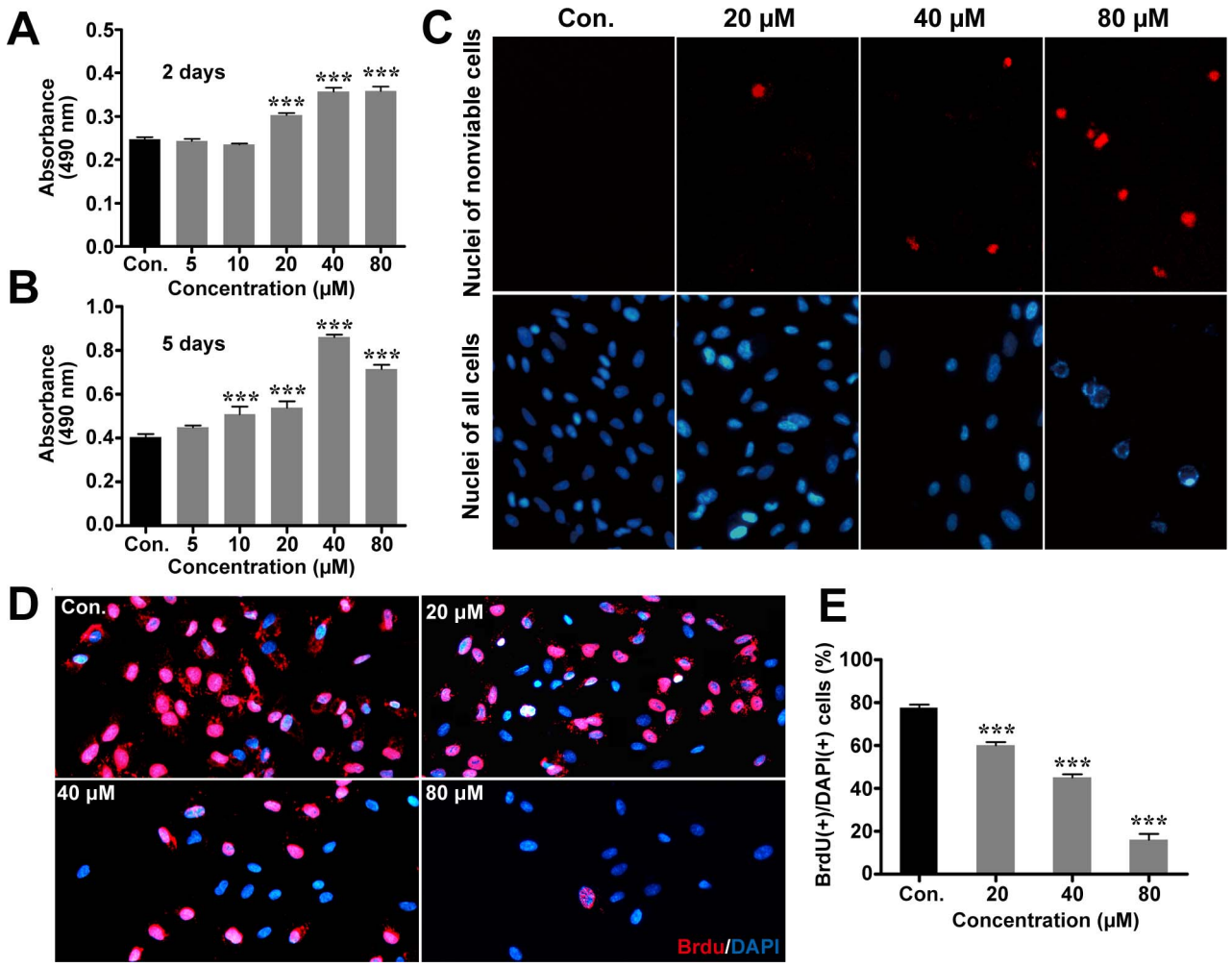

Figure 3. Cytotoxicity and proliferation inhibition induced by atRAL dimer in RPE cells. (**A**, **B**) Lactate dehydrogenase release from cultured RPE cells receiving atRAL dimer. Cells were incubated with atRAL dimer (0, 5, 10, 20, 40, and 80 μM) for 2 (**A**) and 5 (**B**) days in fresh serum-free medium. $^{***}P < 0.001$, significantly different compared with control. (**C**) Fluorescence labeling of the nuclei of membrane-compromised cells. Cultured RPE cells were untreated or exposed to 20, 40, and 80 μM atRAL dimer for 3 days. Microscopic visualization of nonviable cells was accomplished by labeling the nuclei of nonviable cells with Dead Red (Molecular Probes, Invitrogen) and nuclei of all cells with DAPI (*blue*). (**D**) Typical fluorescence photomicrographs of RPE cells stained with BrdU: BrdU, 24 hours after treatment of RPE cells with atRAL dimer (0, 20, 40, and 80 μM), was added to the culture, and the incubation was continued for another 24 hours. Proliferating cells were visualized by BrdU immunofluorescence and total cells were stained with DAPI. (**E**) A statistical chart exhibited the percentage of BrdU (+) cells in DAPI (+) cells. Values were based on counts performed in triplicate wells in each of two independent experiments, with approximately three to five fields counted per well, and were presented as mean ± SEM. $^{***}P < 0.001$.

by 2 N HCl for 30 minutes at 37°C. Then the samples were neutralized by 0.1 M borate buffer for 10 minutes and fixed once again. Following incubation with immunol staining blocking buffer to block nonspecific staining for 30 minutes, cells were treated with anti-BrdU antibody (1:100; Santa Cruz Biotechnology Co., Ltd., Shanghai, China) at 4°C overnight. After three washes with PBS, cells were incubated with Alexa Fluor 594-conjugated AffiniPure Donkey Anti-Mouse IgG (H+L) (1:100 dilution; Jackson ImmunoResearch Laboratories) for 2 hours at 37°C. Finally, cells were counterstained with DAPI and analyzed with the Leica DMI3000B fluorescence microscope (Leica, Wetzlar, Hessen, Germany).

Immunoblot Assays

Human RPE cells (ARPE-19) that underwent treatment with atRAL dimer (0, 20, 40, and 80 μM) for 3 days were harvested from six-well cell culture plates and washed with PBS. Then cells were lysed in ice-cold lysis buffer (RIPA Lysis Buffer; Beyotime) for 5 minutes and centrifuged at 13,000*g* for 5 minutes at 4°C. Protein concentrations in the supernatants were measured using the BCA protein assay kit (Beyotime). Fifty micrograms of proteins in each sample were subjected to SDS-PAGE, and the gels were transferred to 0.2 μm nitrocellulose membranes by electroblotting. Nitrocellulose membranes were exposed to 5 mg/mL nonfat milk for 70 minutes at room temperature with an aim of blocking nonspecific binding, and incubated overnight at 4°C with primary antibodies (Cell Signaling Technology) against Bcl-2 (1:1000 dilution), Bax (1:1000 dilution), Caspase-3 (1:1000 dilution), Tubulin (1:1000 dilution), p-wee1 (1:1000 dilution), Cdc25C (1:1000 dilution), Cyclin B1 (1:1000 dilution), Cdc2 (1:1000 dilution), Chk2 (1:1000 dilution), p53 (1:1000 dilution), p21 (1:1000 dilution), and glyceraldehyde 3-phosphate dehydrogenase (GAPDH) (1:5000 dilution). After being washed with TTBS three times,

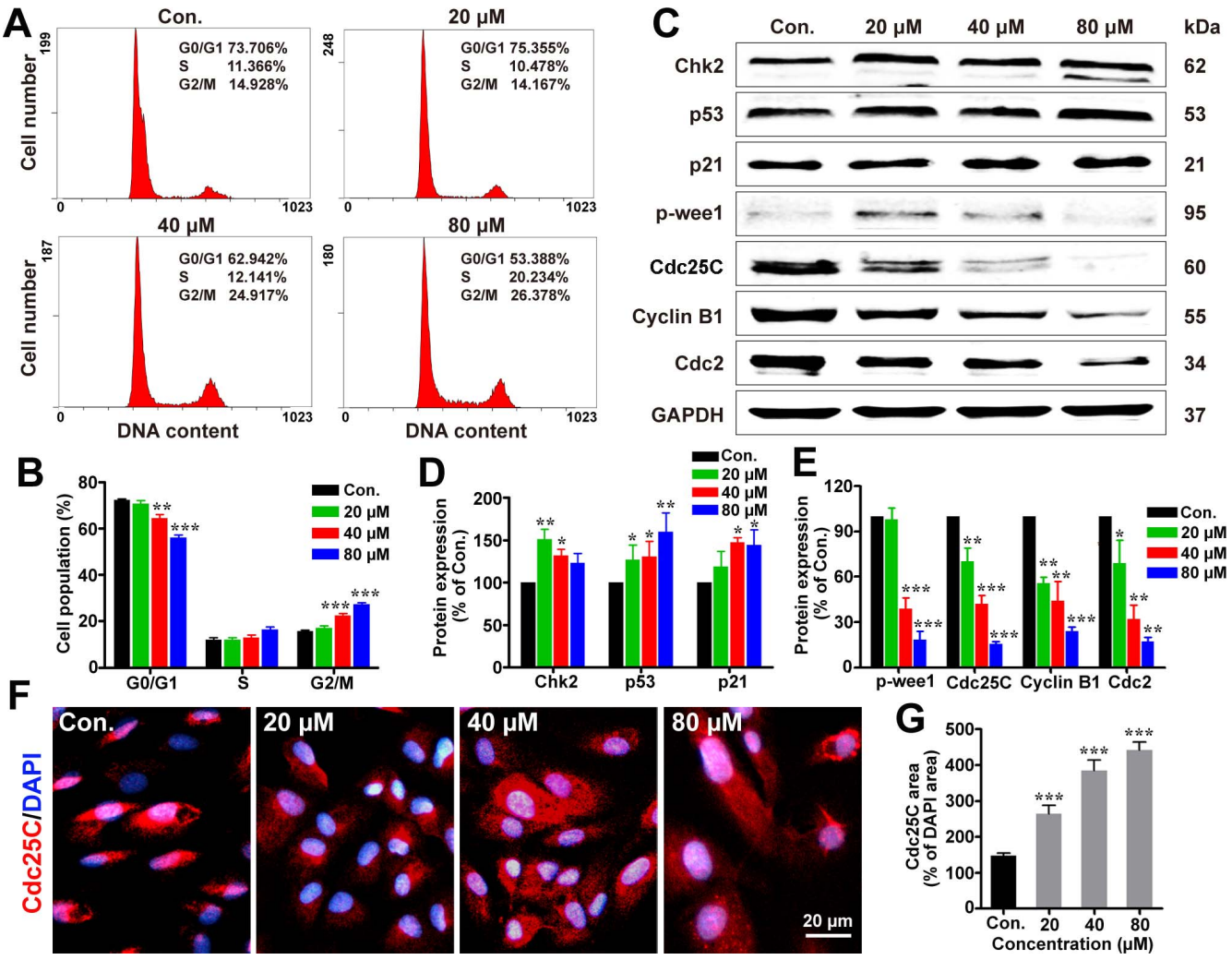

Figure 4. All-*trans*-retinal dimer caused G2/M cell cycle arrest and activated the ATM/ATR-Chk2-p53 signaling pathway. (**A**) Flow cytometry analysis of cell-cycle phase distribution in RPE cells treated with 0, 20, 40, and 80 μM atRAL dimer for 3 days. Cell number shown in the *y* axle indicates peak value of the cell cycle phase. (**B**) Histograms displayed the percentage of cell-cycle distribution. Data were expressed as mean ± SEM from three independent experiments. $^{**}P < 0.01$ and $^{***}P < 0.001$ versus control cells not exposed to atRAL dimer. (**C–E**) Expression levels of cell-cycle–associated proteins Chk2, p53, p21, p-wee1, Cdc25C, Cyclin B1, and Cdc2 were measured by Western blot after treating RPE cells with atRAL dimer for 3 days. The full-length blots are shown in Supplementary Figure S5. Each protein intensity was expressed as mean ± SEM of three independent experiments. $^{*}P < 0.05$, $^{**}P < 0.01$, and $^{***}P < 0.001$. (**F**) Colocalization of Cdc25C protein and the nuclei of RPE cells displayed the atRAL dimer–induced nuclear exclusion of Cdc25C after 2 days; Cdc25C was visualized via immunofluorescence with a specific Cdc25C antibody followed by Alexa Fluor 594-conjugated AffiniPure Donkey Anti-Rabbit IgG (H+L). Nuclear staining was performed with DAPI and is shown in *blue*. (**G**) The area percentage of Cdc25C protein in DAPI was quantified by Image J software (http://imagej.nih.gov/ij/; provided in the public domain by the National Institutes of Health, Bethesda, MD, USA) from three independent experiments. Data were presented as mean ± SEM. $^{***}P < 0.001$ as compared with control cells.

the membranes were incubated with secondary antibodies (IRDye 800/700CW Donkey anti-Rabbit/Mouse; LI-COR, Lincoln, NE, USA) for 2 hours at room temperature. Specific antibody binding was detected by an Odyssey Fc Dual-Mode Imaging System (LI-COR), and band intensity was quantified using the software of Image Studio Lite Version 4.0 (LI-COR). With regard to in vivo expression of apoptosis/cell-cycle-associated proteins, 4-month-old C57BL/6J WT and *Abca4*$^{-/-}$*Rdh8*$^{-/-}$ DKO mouse eyecups without cornea, lens, and vitreous were homogenized in complete EDTA-free protease inhibitor mixture (MAIBIO, Shanghai, China) and centrifuged at 13,000*g* for 5 minutes at 4°C. Protein concentrations in the homogenates were determined by the BCA protein assay kit. Protein extracts from retinal tissues of mouse eyes were tested for protein expression of Bcl-2, Bax, Caspase-3, Cyclin B1, Cdc2, p53, and GAPDH as described above.

Statistical Analysis

All experiments were independently repeated at least three times. Data were analyzed using 1-way ANOVA and Newman-Keuls test for multiple comparisons (Prism 5.0; GraphPad Software, La Jolla, CA, USA), and expressed as mean ± SEM. A *P* value less than 0.05 was considered to be statistically significant.

Results

Quantification, Internalization, Subcellular Location, Cytotoxicity, and Cellular Proliferation Inhibition

The constituents of RPE lipofuscin in eyes of C57BL/6J WT and *Abca4*$^{-/-}$*Rdh8*$^{-/-}$ DKO mice were reexamined. Reverse-phase

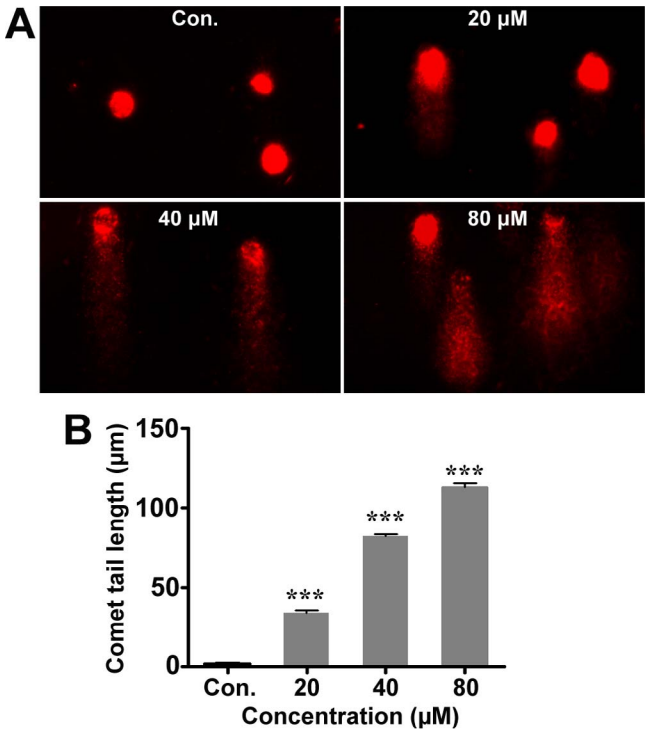

FIGURE 5. Induction of DNA damage by atRAL dimer in RPE cells. (**A**) After 3 days following exposure to 0, 20, 40, and 80 μM atRAL dimer, cells were subjected to the alkaline comet assay for detecting DNA strand breaks. Typical fluorescence photomicrographs of atRAL dimer induced DNA comets stained with EB. (**B**) Quantification of DNA strand breakage at 2 or 3 days after treatment of RPE cells with atRAL dimer at indicated concentrations. Tail moment is indicative of the extent of DNA damage. Data are expressed as mean ± SEM of results in two independent experiments; approximately 50 to 100 nuclei per treatment were randomly selected to measure the comet tail length from the trailing edge of the nucleus to the leading edge of the tail. ***$P < 0.001$ as compared with control cells.

HPLC chromatogram showed a significant peak corresponding to atRAL dimer in a hydrophobic extract derived from six eyes of 6-month-old *Abca4*$^{-/-}$*Rdh8*$^{-/-}$ DKO mice while monitoring eluents at 430 nm (Fig. 1C). We quantified atRAL dimer and A2E in eyes of WT and *Abca4*$^{-/-}$*Rdh8*$^{-/-}$ DKO mice at 2, 4, 6, 8, or 10 months of age. The data indicated that atRAL dimer was remarkably upregulated in *Abca4*$^{-/-}$*Rdh8*$^{-/-}$ DKO mice versus age-matched WT mice (Fig. 1D), as previously reported.[19] Even more strikingly, the amount of atRAL dimer was observed to be much greater than that of A2E in *Abca4*$^{-/-}$*Rdh8*$^{-/-}$ DKO mice (Fig. 1E).

Confocal imaging in the horizontal plane confirmed that exogenously delivered atRAL dimer was internalized by RPE cells in culture (Fig. 2A). Intensity of green autofluorescence from internalized atRAL dimer granules was augmented at concentrations from 5 to 80 μM. Because internalized atRAL dimer was found to be distributed in a punctate perinuclear pattern that is characteristic of lysosomes, we sought to define the intracellular compartmentation of atRAL dimer. Accordingly, cultured RPE cells were simultaneously incubated with atRAL dimer and LysoTracker Red DND, a membrane-diffusible acidophilic fluorophore. On examination by confocal laser scanning microscopy, loads of intracellular granules containing atRAL dimer were observed to colocalize with the LysoTracker probe (Fig. 2B).

To understand the level at which atRAL dimer is tolerated by RPE cells in vitro, we tested the ability of atRAL dimer amassed in RPE cells to perturb membrane integrity; membrane damage was examined by assaying the release of cytoplasmic LDH into culture medium. As shown in Figure 3A, cultured RPE cells exposed to atRAL dimer did not exhibit elevated LDH levels at 5 and 10 μM after 2 days of incubation in fresh serum-free medium, but did display a remarkable increase in LDH levels at concentrations ranging from 20 to 80 μM. When atRAL dimer treatment stretched over 5 days, a significant increase of LDH levels was readily observed with atRAL dimer concentrations starting from 10 μM (Fig. 3B). All-*trans*-retinal dimer–induced cell death was visualized by labeling all cells with DAPI and compromised cells with Dead Red, a membrane-impermeant fluorescent dye. Compared with the control in which cell damage/death did not occur, the percentage of nonviable/dead cells in total cells increased with increasing atRAL dimer exposure concentrations (Fig. 3C). Based on the phenomenon that atRAL dimer substantially decreased count and density of RPE cells (Fig. 3C), we inferred that atRAL dimer likely inhibited natural growth of RPE cells. Accordingly, the proliferating cells were examined by labeling with BrdU immunofluorescence after incubating atRAL dimer with RPE cells. Indeed, nearly 80% of control cells were proliferating, but atRAL dimer–laden RPE cells were significantly inhibited to reproduce in a concentration-dependent manner (Fig. 3D). By counting cell number in triplicate wells in each of two experiments with three to five fields per well, the rates of BrdU (+) cells/DAPI (+) cells clearly decreased with increasing atRAL dimer exposure concentrations (Fig. 3E), thereby confirming the occurrence of RPE cell proliferation suppression.

All-*Trans*-Retinal Dimer Induces DNA Strand Breaks, and Triggers Cell-Cycle Arrest at the G2/M Phase by Activating the ATM/ATR-Chk2-p53 Signaling Pathway

To further examine the mechanism by which atRAL dimer may inhibit proliferation of RPE cells, we investigated the effects of atRAL dimer on cell cycle. Retinal pigment epithelium cells were incubated with serial concentrations of atRAL dimer for 3 days, stained with PI, and finally evaluated by flow cytometry (Fig. 4A). As expected, starting at 40 μM, atRAL dimer induced cell-cycle arrest in the G2/M phase (Fig. 4B).

To obtain further insight into the mechanism of atRAL dimer–induced RPE cell-cycle arrest, we studied the expression of several cell-cycle–associated regulators by a Western blotting assay as well as an immunofluorescence staining of Cdc25C, a tyrosine phosphatase that plays a key role in the regulation of cell division.[23] Once Cdc25C is phosphorylated at the site of Ser^{216} under the action of Chk2, phosphorylated Cdc25C will bind to 14-3-3 and then block mitotic entry under normal conditions and after DNA damage.[24,25] In the current study, immunofluorescence analysis with anti-Cdc25C antibody revealed that atRAL dimer clearly triggered the nuclear exclusion of Cdc25C in RPE cells at concentrations starting from 20 μM (Figs. 4F, 4G). With immunoblot assays, RPE cells treated with atRAL dimer significantly exhibited an increase in protein levels of Chk2, p53, and p21, but the expression of Cdc25C, Cyclin B1, Cdc2, and p-wee1 was clearly decreased in a concentration-dependent manner (Figs. 4C–E). It has been previously reported that Chk2 and p53 are activated via the ataxia telangiectasia–mutated (ATM)/ATM and Rad3-related (ATR) signaling pathway.[26] p21, a p53 downstream effector, serves as an inhibitor of Cyclin B1-Cdc2 complexes that control the G2/M transition.[27] As depicted in Figure 4C, the overexpression of p53 and p21 in atRAL dimer–laden RPE cells impeded the activation of the Cyclin B1-Cdc2 complexes,

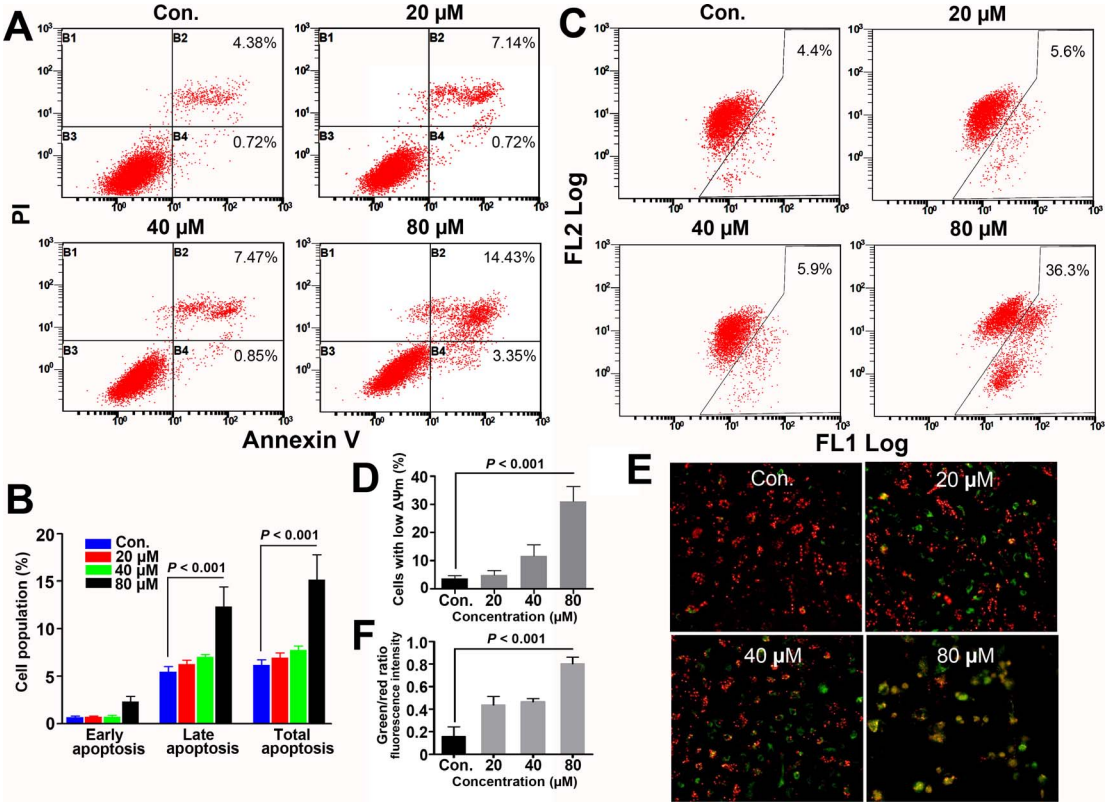

Figure 6. Evidence that atRAL dimer induced apoptosis in RPE cells. (**A**) Flow cytometry analysis via Annexin V/PI staining was used to identify apoptosis after incubations of RPE cells with atRAL dimer (0, 20, 40, and 80 μM) for 3 days. (**B**) A bar graph manifested the percentage of cells at different stages of the apoptotic program; mean ± SEM from three independent experiments. (**C**) Typical dot plots of MMP changes in RPE cells treated with atRAL dimer (0, 20, 40, and 80 μM) for 3 days were generated by JC-1 staining flow cytometry. (**D**) A bar chart displayed the percentage of cells with low MMP (ΔΨm); mean ± SEM of three independent experiments. (**E**) Representative fluorescence photomicrographs of in situ JC-1 staining output by the inverted fluorescence microscopy. *Scale bars*: 100 μm. (**F**) Green/red ratio was quantified from three dependent experiments by Image Pro Plus software (Media Cybernetics, Rockville, MD, USA). Data were presented as mean ± SEM. $^{***}P < 0.001$ as compared with control cells.

which was associated with the G2/M cell-cycle arrest. Taken together, the data suggest that atRAL dimer induces the G2/M phase arrest via the ATM/ATR-Chk2-p53 pathway. Given that p53 and Chk2 will be activated by the ATM/ATR signaling pathway when DNA damage takes place within RPE cells, atRAL dimer–induced direct DNA strand breaks was tested by means of single-cell gel electrophoresis (comet assay). Comet assay was carried out under alkaline conditions that permit damaged DNA to be drawn out into a comet tail when subjected to an electrical field. Indeed, the presence of DNA strand breaks was visualized by the emergence of comet tails from the nuclei of atRAL dimer–laden cells (Fig. 5A). By contrast, the nuclei of control cells remained spherical. Tail moment, a parameter whose magnitude reflects the frequency of DNA strand breaks per nucleus,[28–30] was remarkably elevated in atRAL dimer–fed cells, indicative of DNA damage response; the increased magnitude in tail moment was found to be dependent on exposure concentrations of atRAL dimer (Fig. 5B). The average comet tail moments of RPE cells exposed to 20-, 40-, and 80-μM atRAL dimer, were measured as 34.14, 82.01, and 113.30 μm, respectively.

All-*Trans*-Retinal Dimer Causes Apoptosis, and Activates the Mitochondria-Dependent Pathway in RPE Cells

To assess whether atRAL dimer exhibited a proapoptotic effect on RPE cells, flow cytometry analysis via Annexin V/PI staining was performed. A total of Annexin V+/PI– and Annexin V+/PI+ cells indicate cell death through both early- and late-stage apoptosis. After treatment with atRAL dimer for 3 days, the percentage of apoptotic cells increased concentration-dependently (Fig. 6A), and was significant at the concentration of 80 μM versus the control (Fig. 6B). Disruption of ΔΨm is an early event in the process of apoptosis in mammalian cells,[31] reflecting the mitochondrial membrane permeability transition. Results of staining with the ΔΨm sensing dye JC-1 demonstrated that the untreated cells exhibited an intact ΔΨm, but atRAL dimer exposure significantly induced ΔΨm loss in RPE cells at the concentration of 80 μM, as indicated by a shift in JC-1 fluorescence from aggregate (red) to monomer (green) (Figs. 6E, 6F). To further corroborate this finding, we evaluated the fluorescence of JC-1 with flow cytometry and found that, compared with control cells (4.4%), the number of cells with reduction of ΔΨm was not significantly increased after 20 μM (5.6%) and 40 μM (5.9%) atRAL dimer exposures for 3 days, but was apparently raised following 80 μM (36.3%) atRAL dimer treatment (Fig. 6C), consistent with quantitative data on the amount of low ΔΨm cells from three independent experiments (Fig. 6D). On examination by confocal laser scanning microscopy, treatment of RPE cells with atRAL dimer clearly inflicted the release of cytochrome *c* from mitochondria to the cytoplasm versus control cells that retained cytochrome *c* in the mitochondria (Fig. 7A). In addition, we observed a clear upregulation of the cleaved fragment of caspase-3 after 80 μM atRAL dimer exposure, which was accompanied by a

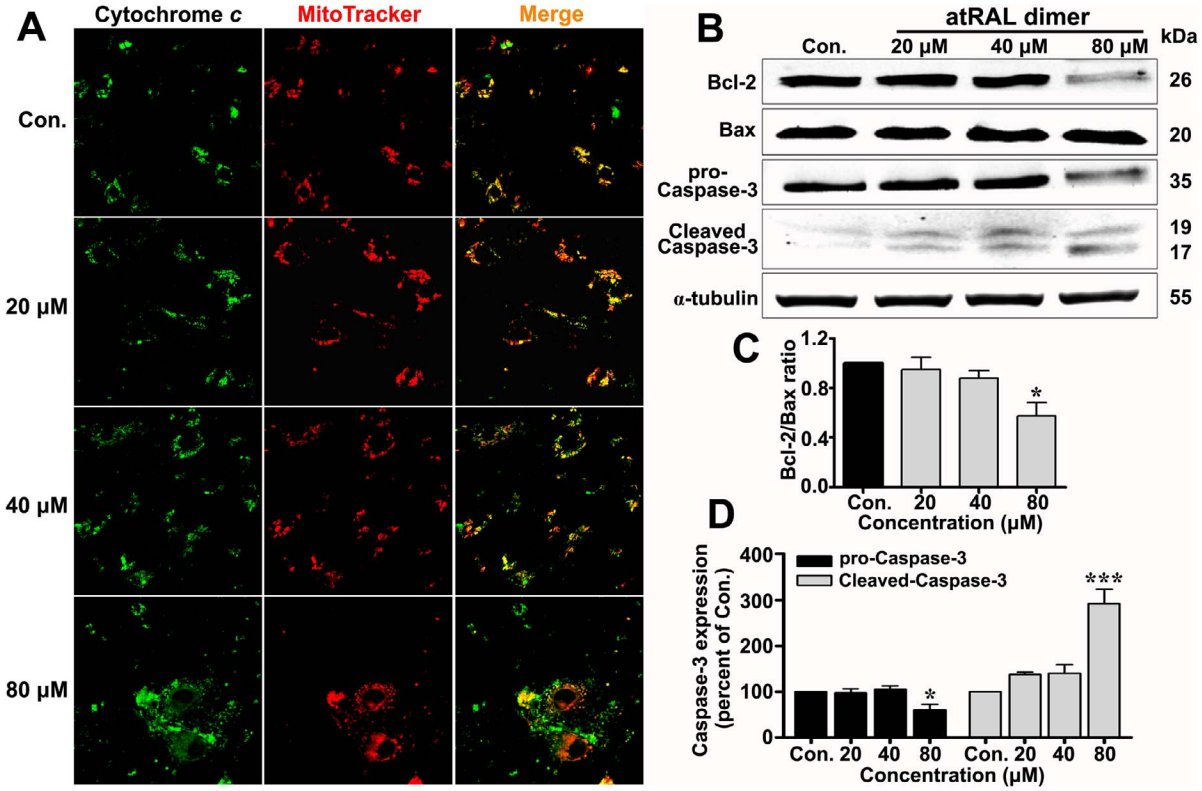

Figure 7. All-*trans*-retinal dimer induced cytochrome *c* release from mitochondria and expression changes of typical apoptosis regulatory proteins within RPE cells. (**A**) Retinal pigment epithelial cells, 3 days after exposing to 0, 20, 40, and 80 μM atRAL dimer, were examined by immunofluorescence for cytochrome *c* localization. The distribution of cytochrome *c* (*green*) and MitoTracker (*red*) by confocal fluorescence microscopy exhibited the release of cytochrome *c* into the cytosol. (**B**) Protein expression of Bcl-2, Bax, and Caspase-3, 3 days after cells were treated with atRAL dimer (0, 20, 40, and 80 μM), was determined using Western blot, and quantified by Image Studio Lite Version 4.0 software. The full-length blots are presented in Supplementary Figure S6. (**C**) The protein expression ratio of Bcl-2 to Bax was presented as fold change in treated cells compared with control cells. Note that the normalization for band intensity of Bcl-2 and Bax against that of α-tubulin was individually made before calculating the Bcl-2/Bax ratio. Each value represents mean ± SEM from three independent experiments. $^{*}P < 0.05$. (**D**) The protein expression level of caspase-3 in atRAL dimer–treated cells versus control cells, including pro-caspase-3 and cleaved caspase-3. The data are shown as mean ± SEM; $^{*}P < 0.05$, $^{***}P < 0.001$.

reduction in protein expression of pro-caspase-3 (Figs. 7B, 7D). To further identify apoptosis onset in RPE cells via activation of the mitochondrial pathway, Western blot analysis also was used to detect antiapoptotic mitochondrial protein Bcl-2 and proapoptotic mitochondrial protein Bax, and revealed that atRAL dimer concentration-dependently caused downregulation of Bcl-2 and upregulation of Bax (Fig. 7B). By comparison with control cells, the ratio of Bcl-2/Bax decreased with increasing atRAL dimer exposure concentrations, and was significant at the concentration of 80 μM (Fig. 7C).

p53-Dependent Apoptosis and G2/M Phase Cell-Cycle Arrest Are Detected in the RPE of *Abca4*$^{-/-}$*Rdh8*$^{-/-}$ DKO Mice

Considering that an increased amount of atRAL dimer was detected in eyes of *Abca4*$^{-/-}$*Rdh8*$^{-/-}$ DKO mice versus WT mice (Fig. 1D), in vivo expression of several proteins correlated with apoptosis and G2/M phase arrest of the cell cycle was examined (Figs. 8A, 8D). As expected, quantitative immunoblot analysis showed that p53 protein exhibited a 1.7-fold increase in the RPE of 4-month-old *Abca4*$^{-/-}$*Rdh8*$^{-/-}$ DKO mice compared with age-matched WT mice (Fig. 8B). Immunoblotting analysis of the RPE from *Abca4*$^{-/-}$*Rdh8*$^{-/-}$ DKO mice at age 4 months demonstrated the upregulation of Bax protein and downregulation of Bcl-2 protein versus that of the RPE dissected from age-matched WT mice (Fig. 8A), thus giving rise to a 93.94% decrease in the ratio of Bcl-2/Bax (Fig. 8C). Furthermore, protein expression of cleaved caspase-3 in the RPE of *Abca4*$^{-/-}$*Rdh8*$^{-/-}$ DKO mice was visibly raised, along with a reduction of the pro-caspase-3 protein expression (Fig. 8A). On the other hand, in vivo expression of Cyclin B1 and Cdc2 required for the G2/M phase transition of the cell cycle was clearly altered in the RPE of *Abca4*$^{-/-}$*Rdh8*$^{-/-}$ DKO mice. We observed an obvious upregulation of Cyclin B1, as well as an apparent downregulation of Cdc2 in the RPE of 4-month-old *Abca4*$^{-/-}$*Rdh8*$^{-/-}$ DKO mice versus that of age-matched WT mice (Fig. 8D). Quantitative immunoblot analysis demonstrated that there was an approximately 60% decline in the Cdc2 protein expression level in the RPE of *Abca4*$^{-/-}$*Rdh8*$^{-/-}$ DKO mice at 4 months of age compared with age-matched WT mice (Fig. 8E), whereas expression level of Cyclin B1 protein showed an approximately 2-fold increase in the RPE of *Abca4*$^{-/-}$*Rdh8*$^{-/-}$ DKO mice (Fig. 8F).

Discussion

There is a growing body of evidence to substantiate that A2E is a representative and rich aging pigment in the RPE lipofuscin.[11,15,32] A2E has been considered to cause damage to RPE cells, including autophagic response,[33] lysosomal alkalinization,[34] pro-apoptotic protein detachment from mitochondria,[35]

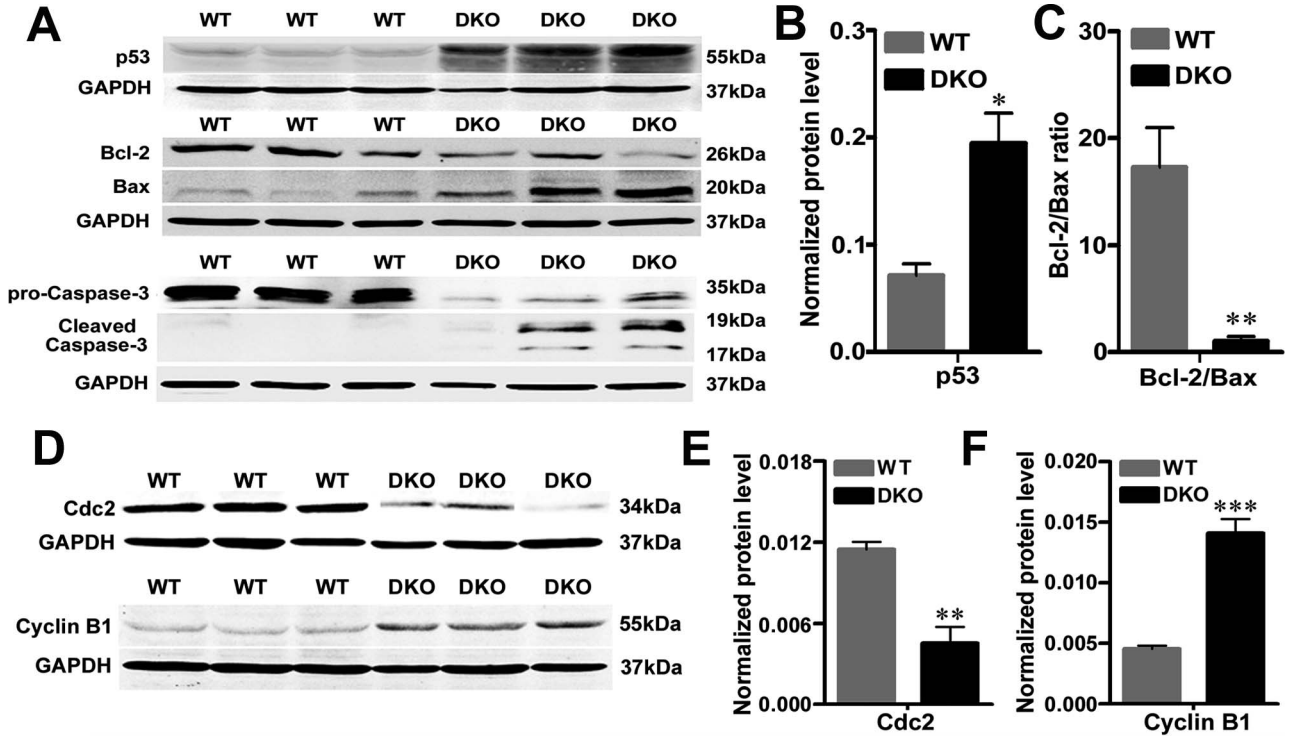

Figure 8. Activation of p53-dependpent apoptosis and abnormal expression of key cell-cycle proteins Cdc2 and Cyclin B1 in the RPE of *Abca4*$^{-/-}$*Rdh8*$^{-/-}$ DKO mice. (**A**) Representative immunoblots for p53, Bcl-2, Bax, Caspase-3, and GAPDH protein from RPE homogenates (60 μg per lane) of WT and *Abca4*$^{-/-}$*Rdh8*$^{-/-}$ DKO mice at 4 months of age. The full-length blots are shown in Supplementary Figure S7. (**B**, **C**) Expression levels of p53, Bcl-2, and Bax protein in the RPE of WT and *Abca4*$^{-/-}$*Rdh8*$^{-/-}$ DKO mice were quantified using the Image Studio Lite software, and normalized to that of GAPDH protein serving as the internal control. $n = 6$, $^{*}P < 0.05$ and $^{**}P < 0.01$ versus WT mice. (**D**) Typical bands of Cdc2, Cyclin B1, and GAPDH protein from RPE homogenates (60 μg per lane) of WT and *Abca4*$^{-/-}$*Rdh8*$^{-/-}$ DKO mice at 4 months of age. The full-length blots are presented in Supplementary Figure S7. (**E**, **F**) Expression levels of Cdc2 and Cyclin B1 protein in the RPE of WT and *Abca4*$^{-/-}$*Rdh8*$^{-/-}$ DKO mice were measured using the Image Studio Lite software and normalized to that of GAPDH protein. $n = 6$, $^{**}P < 0.01$ and $^{***}P < 0.001$ versus WT mice.

and inflammatory chemokine and cytokine production[33,36] as well as a detergent-like effect on the cytomembrane.[37] By contrast, atRAL dimer is barely detected in eyes of WT mice compared with A2E.[19] However, the amount of atRAL dimer dramatically increased in eyes of *Abca4*$^{-/-}$*Rdh8*$^{-/-}$ DKO mice versus WT mice (Fig. 1D),[19] and was even much greater than that of A2E in eyes of *Abca4*$^{-/-}$*Rdh8*$^{-/-}$ DKO mice (Fig. 1E). *Abca4*$^{-/-}$*Rdh8*$^{-/-}$ DKO mice are established by cross-breeding *Abca4*$^{-/-}$ mice, a model of recessive Stargardt disease,[38] with *Rdh8*$^{-/-}$ mice. In the DKO mouse RPE cells, the deposition of A2E and atRAL dimer was already apparent by 2 months of age, and although it continued to increase until approximately 6 months of age (atRAL dimer, 93.34 ± 4.828 pmol/eye; A2E, 21.18 ± 1.129 pmol/eye), thereafter it declined (Fig. 1E). This trend of change in the quantity of endogenous atRAL dimer and A2E is possibly because the attenuation in the rate of the visual cycle after the age of 6 months slows their accumulation in *Abca4*$^{-/-}$*Rdh8*$^{-/-}$ DKO mice, whereas continuous light-induced oxidation and cleavage leads to the decrease in levels of atRAL dimer and A2E to a certain degree.[39–41] Another possible explanation for the phenomenon is due to exacerbated loss of photoreceptors and removal of atrophic RPE cells in *Abca4*$^{-/-}$*Rdh8*$^{-/-}$ DKO mice aged older than 6 months. The finding is supported by early studies regarding changes in the amount of RPE lipofuscin in humans with age.[42–45]

Using HPLC to quantify atRAL dimer within cultured RPE cells, we found that the amount of atRAL dimer internalized by the cells varied with the concentration of atRAL dimer in the medium and with the incubation period, and tentatively estimated that 6% to 13% of atRAL dimer in the medium was internalized by the RPE cells. By contrast, Sparrow and coworkers[37] demonstrated that an estimated 5% to 10% of A2E in the medium is internalized by the RPE cells, and compared the level of A2E internalized by cultured RPE cells with an estimated amount of endogenous A2E in RPE cells isolated from healthy human donor eyes at ages ranging from 58 to 79, thus concluding that 10- to 25-μM concentrations of A2E in the medium are required to achieve intracellular levels that approximate those amounts of A2E measured in human RPE. In the present study, HPLC quantification of atRAL dimer and A2E in eyes of *Abca4*$^{-/-}$*Rdh8*$^{-/-}$ DKO mice revealed that the amount of atRAL dimer is more than four times greater than that of A2E (Fig. 1E). Accordingly, it may be physiologically relevant for the concentrations at which atRAL dimer is presented in the cell-based experiments of this work.

Although A2E and atRAL dimer are both derived from atRAL or 11-*cis*-retinal,[9,14,46] there is a distinct difference between them on the chemical structure. A2E contains a pyridinium ring on which a positive charge on the nitrogen atom linked to a saturated alcohol group (Fig. 1A), whereas atRAL dimer is a nonpyridinium bisretinoid with a simpler cyclohexadiene ring that is attached by an aldehyde moiety (Fig. 1B). Moreover, atRAL dimer is much more photosensitive than A2E.[41] Previous evidence demonstrated the inability of A2E to damage DNA of RPE cells at a 20-μM concentration in the medium.[47] Conversely, comet assay revealed that atRAL dimer significantly induced DNA damage on RPE cells at concentrations starting from 20 μM (Fig. 5).

Although it is clear that there are levels of atRAL dimer that are tolerated by RPE cells, intracellular concentrations can be reached above which atRAL dimer is damaging to RPE cells. As depicted in Figure 9, we did verify that atRAL dimer inhibited

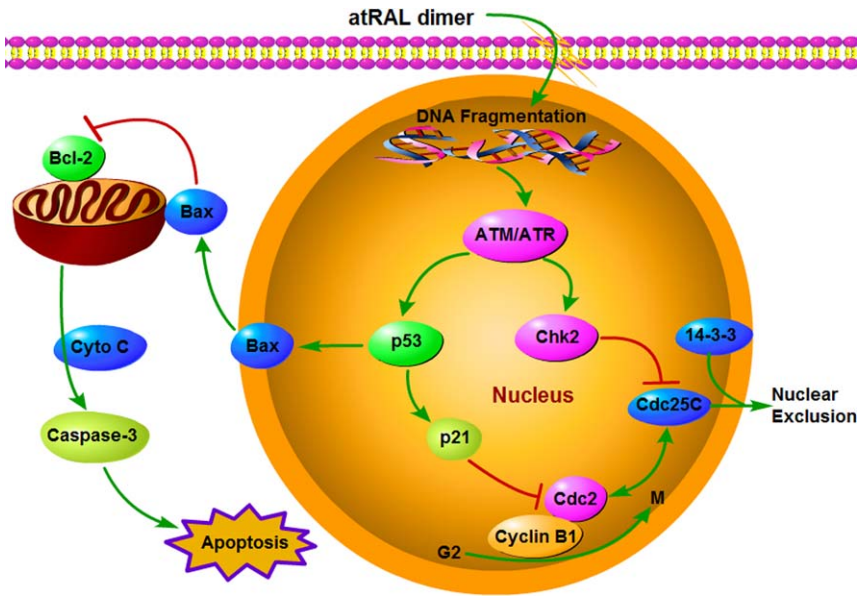

Figure 9. Mechanism for atRAL dimer induced proliferation inhibition and apoptosis of RPE cells. When endogenously produced to a critical level, atRAL dimer, an indigestible lipofuscin pigment in the RPE, triggers a DNA damage response and activates the ATM/ATR-Chk2-p53 pathway. Chk2 can phosphorylate Cdc25C and thereby inhibit the Cdc25C-mediated activation of Cyclin B1-Cdc2 complexes, which is essential for the G2/M phase transition of the cell cycle. Phosphorylation of Cdc25C by Chk2 creates a binding site for the 14-3-3 family of phosphoserine binding proteins, and 14-3-3 proteins can regulate Cdc25C by sequestering it from the nucleus to the cytoplasm. Furthermore, upregulation of p53 also activates p21, an inhibitor of activation of the Cyclin B1-Cdc2 complexes. Taken together, atRAL dimer–triggered suppression of cell proliferation is likely an important cause of RPE degeneration. On the other land, DNA damage–induced activation of p53 by atRAL dimer in the RPE results in aberrant expression of the apoptosis-related proteins Bax and Bcl-2, the release of cytochrome *c* from mitochondria, and Caspase-3 activation, indicating that atRAL dimer–provoked RPE degeneration is also involved with the mitochondrial apoptosis pathway.

RPE cell proliferation (Figs. 3D, 3E) and induced cell-cycle arrest at the G2/M phase via activation of the ATM/ATR-Chk2-p53 signaling pathway (Fig. 4), as well as caused DNA damage (Fig. 5) and mitochondrion-associated apoptosis in RPE cells (Figs. 6, 7). In addition, although atRAL dimer could have clearly inflicted membrane damage (Figs. 3A, 3B), we observed that LDH levels following exposure of RPE cells to atRAL dimer for 5 days, first increased in a concentration-dependent manner, but gave a trend to decrease at 80 μM (Fig. 3B). Moreover, in contrast to the control group, DAPI-stained cells showed a significant decrease in the count and density with increasing atRAL dimer exposure concentrations (Figs. 3C, 3D). These phenomena are likely caused by the occurrence of proliferation inhibition in RPE cells induced by atRAL dimer, which leads to a rapid reduction in the number of cells. Evidence from immunoblot studies on the RPE of *Abca4*$^{-/-}$*Rdh8*$^{-/-}$ DKO mice manifested that excess buildup of atRAL dimer, at least in part, contributes to the degeneration of the RPE in vivo (Fig. 8).

The *rd8* mutation of the *Crb1* gene is unexpectedly detected in vendor strains of C57BL/6N mice.[22] Thus, it is suspected that *Crb1*^{rd8} mutation might be responsible for the retinal degeneration in several mutant mouse models exhibiting AMD-like lesions.[48,49] Here we found that *Crb1*^{rd8} mutation was present in *Abca4*$^{-/-}$*Rdh8*$^{-/-}$ DKO mice (Supplementary Figs. S8A, S8B). However, *Crb1*^{rd8} mice usually exhibit retinal folds and pseudorosettes at 2 months of age,[50] which are not observed in *Abca4*$^{-/-}$*Rdh8*$^{-/-}$ DKO mice. In contrast, *Abca4*$^{-/-}$*Rdh8*$^{-/-}$ DKO mice used in this study develop lipofuscin, drusen, basal laminar deposits, Bruch's membrane thickening, and choroidal neovascularization,[19] which are cardinal to AMD pathology but not shown in *Crb1*^{rd8} mutant mice. In *Crb1*^{rd8} mutant mice, the shortening of photoreceptor inner and outer segments is observed within 2 weeks after birth, suggestive of a developmental defect.[50] Distinctively, retinal structure is normal in *Abca4*$^{-/-}$*Rdh8*$^{-/-}$ DKO mice by 3 weeks of age, and the phenotypes are aggravated with age. Even more importantly, retinal lesions are exacerbated by light exposure, and rescued by the administration of retinylamine, a visual cycle inhibitor, implying that AMD-like lesions in *Abca4*$^{-/-}$*Rdh8*$^{-/-}$ DKO mice are more likely due to the abnormal accumulation of atRAL and its derived products.[19] Therefore, we concluded that the phenotypes observed in the RPE of *Abca4*$^{-/-}$*Rdh8*$^{-/-}$ DKO mice were largely due to retinoid dysregulation. On the other hand, deletion of CRB1 could alter cell-cycle distribution of retinal progenitor cells and thereby more cells reside in the G2/M phases,[51] suggesting that *Crb1* mutation may affect the expression levels of cell-cycle–related proteins. In this study, we have shown that the expression of Cyclin B1 and Cdc2, two key cell-cycle proteins, is significantly altered in atRAL dimer–laden RPE cells (Fig. 4C) and the RPE of *Abca4*$^{-/-}$*Rdh8*$^{-/-}$ DKO mice (Figs. 8D–F). The expression of Cyclin B1 was decreased in atRAL dimer–treated RPE cells (Figs. 4C, 4E), but increased in the RPE of *Abca4*$^{-/-}$*Rdh8*$^{-/-}$ DKO mice (Figs. 8D, 8F). To exclude the possibility that *Crb1*^{rd8} might contribute to the difference of Cyclin B1 expression in vitro and in vivo, its protein level in the RPE of C57BL/6J, C57BL/6N and *Abca4*$^{-/-}$*Rdh8*$^{-/-}$ DKO mice was measured by Western blot (Supplementary Fig. S8C), which indicated that the increase of Cyclin B1 in the RPE of *Abca4*$^{-/-}$*Rdh8*$^{-/-}$ DKO mice was not due to the mutation in the *Crb1* gene. Nevertheless, whether *rd8* mutation partially accounts for the retinal degeneration observed in *Abca4*$^{-/-}$*Rdh8*$^{-/-}$ DKO mice is worth further investigation. Furthermore, the expression of Cdc2 was downregulated both in vitro (Figs. 4C, 4E) and in vivo (Figs. 8D, 8E), suggesting that the formation of Cyclin B1-Cdc2 complexes was positively suffocated. Reduced formation of Cyclin B1-Cdc2 complexes would suppress progression of the cell cycle from the G2 phase to the M phase.[52]

Delayed clearance of atRAL in the photoreceptors would result in excess accumulation of atRAL dimer in the RPE.[19] The finding that atRAL dimer is much more abundant than A2E in eyes of *Abca4*$^{-/-}$*Rdh8*$^{-/-}$ DKO mice reveals potential importance of atRAL dimer in the RPE degeneration. Most recently, we reported that initially, the conversion of atRAL to atRAL dimer in the retina is likely a protective pathway that detoxifies free atRAL with a highly active aldehyde moiety[53]; however, when atRAL dimer accumulated beyond a critical level, it surely provoked adverse effects on the RPE. This work expands the understanding of different biological properties of atRAL dimer, and may make it as a potential target of gene-based and drug therapies that aim to alleviate age-dependent RPE degeneration.

Acknowledgments

Supported in part by China National Natural Science Foundation Grants 81570857 (YW) and 81271018 (YW); the Fundamental Research Funds for the Central Universities grant (YW); and Natural Science Foundation of Fujian Province Grant 2016J01412 (YL).

Disclosure: **J. Zhao**, None; **Y. Liao**, None; **J. Chen**, None; **X. Dong**, None; **Z. Gao**, None; **H. Zhang**, None; **X. Wu**, None; **Z. Liu**, None; **Y. Wu**, None

References

1. Friedman DS, O'Colmain BJ, Muñoz B, et al. Prevalence of age-related macular degeneration in the United States. *Arch Ophthalmol*. 2004;122:564–572.
2. Gehrs KM, Anderson DH, Johnson LV, Hageman GS. Age related macular degeneration: emerging pathogenetic and therapeutic concepts. *Ann Med*. 2006;38:450–471.
3. Rein DB, Wittenborn JS, Zhang X, Honeycutt AA, Lesesne SB, Saaddine J. Forecasting age-related macular degeneration through the year 2050. The potential impact of new treatments. *Arch Ophthalmol*. 2009;127:533–540.
4. Newman AM, Gallo NB, Hancox LS, et al. Systems-level analysis of age-related macular degeneration reveals global biomarkers and phenotype-specific functional networks. *Genome Med*. 20124:16.
5. Kennedy CJ, Rakoczy PE, Constable IJ. Lipofuscin of the retinal pigment epithelium: a review. *Eye*. 1995;9:763–771.
6. Dorey C, Wu G, Ebenstein D, Garsd A, Weiter J. Cell loss in the aging retina. Relationship to lipofuscin accumulation and macular degeneration. *Invest Ophthalmol Vis Sci*. 1989;30:1691–1699.
7. Sparrow JR, Boulton M. RPE lipofuscin and its role in retinal pathobiology. *Exp Eye Res*. 2005;80:595–606.
8. Steinberg RH. Interactions between the retinal pigment epithelium and the neural retina. *Doc Ophthalmol*. 1985;60:327–346.
9. Liu J, Itagaki Y, Ben-Shabat S, Nakanishi K, Sparrow JR. The biosynthesis of A2E, a fluorophore of aging retina, involves the formation of the precursor, A2-PE, in the photoreceptor outer segment membrane. *J Biol Chem*. 2000;275:29354–29360.
10. Ben-Shabat S, Parish CA, Vollmer HR, et al. Biosynthetic studies of A2E, a major fluorophore of retinal pigment epithelial lipofuscin. *J Biol Chem*. 2002;277:7183–7190.
11. Sakai N, Decatur J, Nakanishi K. Ocular age pigment "A2-E": an unprecedented pyridinium bisretinoid. *J Am Chem Soc*. 1996;118:1559–1560.
12. Parish CA, Hashimoto M, Nakanishi K, Dillon J, Sparrow J. Isolation and one-step preparation of A2E and *iso*-A2E, fluorophores from human retinal pigment epithelium. *Proc Natl Acad Sci U S A*. 1998;95:14609–14613.
13. Li J, Yao K, Yu X, et al. Identification of a novel lipofuscin pigment (iisoA2E) in retina and its effects in the retinal pigment epithelial cells. *J Biol Chem*. 2013;288:35671–35682.
14. Fishkin NE, Sparrow JR, Allikmets R, Nakanishi K. Isolation and characterization of a retinal pigment epithelial cell fluorophore: an all-*trans*-retinal dimer conjugate. *Proc Natl Acad Sci U S A*. 2005;102:7091–7096.
15. Wu Y, Fishkin NE, Pande A, Pande J, Sparrow JR. Novel lipofuscin bisretinoids prominent in human retina and in a model of recessive Stargardt disease. *J Biol Chem*. 2009;284:20155–20166.
16. Wu Y, Jin Q, Yao K, et al. Retinal metabolism in humans induces the formation of an unprecedented lipofuscin fluorophore 'pdA2E.' *Biochem J*. 2014;460:343–352.
17. Zhao J, Yao K, Jin Q, et al. Preparative and biosynthetic insights into pdA2E and *iso*pdA2E, retinal-derived fluorophores of retinal pigment epithelial lipofuscin. *Invest Ophthalmol Vis Sci*. 2014;55:8241–8250.
18. Eldred GE, Katz ML. Fluorophores of the human retinal pigment opithelium: separation and spectral characterization. *Exp Eye Res*. 1988;47:71–86.
19. Maeda A, Maeda T, Golczak M, Palczewski K. Retinopathy in mice induced by disrupted all-*trans*-retinal clearance. *J Biol Chem*. 2008;283:26684–26693.
20. Maeda A, Maeda T, Golczak M, et al. Involvement of all-*trans*-retinal in acute light-induced retinopathy of mice. *J Biol Chem*. 2009;284:15173–15183.
21. Maeda A, Golczak M, Chen Y, et al. Primary amines protect against retinal degeneration in mouse models of retinopathies. *Nat Chem Biol*. 2011;8:170–178.
22. Mattapallil MJ, Wawrousek EF, Chan CC, et al. The Rd8 mutation of the Crb1 gene is present in vendor lines of C57BL/6N mice and embryonic stem cells, and confounds ocular induced mutant phenotypes. *Invest Ophthalmol Vis Sci*. 2012;53:2921–2927.
23. Hoffmann I, Clarke PR, Marcote MJ, Karsenti E, Draetta G. Phosphorylation and activation of human cdc25-C by cdc2-cyclin B and its involvement in the self-amplification of MPF at mitosis. *EMBO J*. 1993;12:53–63.
24. Peng CY, Graves PR, Thoma RS, Wu Z, Shaw AS, Piwnica-Worms H. Mitotic and G2 checkpoint control: regulation of 14–3–3 protein binding by phosphorylation of Cdc25C on serine-216. *Science*. 1997;277:1501–1505.
25. Bulavin DV, Higashimoto Y, Demidenko ZN, et al. Dual phosphorylation controls Cdc25 phosphatases and mitotic entry. *Nat Cell Biol*. 2003;5:545–551.
26. Hirao A, Kong YY, Matsuoka S, et al. DNA damage-induced activation of p53 by the checkpoint kinase Chk2. *Science*. 2000;287:1824–1827.
27. Bunz F, Dutriaux A, Lengauer C, et al. Requirement for p53 and p21 to sustain G2 arrest after DNA damage. *Science*. 1998;282:1497–1501.
28. Fairbairn DW, Olive PL, O'Neill KL. The comet assay: a comprehensive review. *Mutat Res*. 1995;339:37–59.
29. Green ML, Lowe JE, Delaney CA, Green IC. Comet assay to detect nitric oxide-dependent DNA damage in mammalian cells. *Methods Enzymol*. 1996;269:243–265.
30. McCarthy PJ, Sweetman SF, Mckenna PG, McKelvey-Martin VJ. Evaluation of manual and image analysis quantification of DNA damage in the alkaline comet assay. *Mutagenesis*. 1997;12:209–214.
31. Zhang X, Wu J, Dou Y, et al. Asiatic acid protects primary neurons against C2-ceramide-induced apoptosis. *Eur J Pharmacol*. 2012;679:51–59.
32. Eldred GE, Lasky MR. Retinal age pigments generated by self-assembling lysosomotrophic detergents. *Nature*. 1993;361:724–726.

Investigative Ophthalmology & Visual Science

33. Zhang J, Bai Y, Huang L, et al. Protective effect of autophagy on human retinal pigment epithelial cells against lipofuscin fluorophore A2E: implications for age-related macular degeneration. *Cell Death Dis*. 2015;6:e1972.
34. Holz FG, Schütt F, Kopitz J, et al. Inhibition of lysosomal degradative functions in RPE cells by a retinoid component of lipofuscin. *Invest Ophthalmol Vis Sci*. 1999;40:737–743.
35. Suter M, Remé C, Grimm C, et al. Age-related macular degeneration. The lipofusion component *N*-retinyl-*N*-retinylidene ethanolamine detaches proapoptotic proteins from mitochondria and induces apoptosis in mammalian retinal pigment epithelial cells. *J Biol Chem*. 2000;275:39625–39630.
36. Anderson OA, Finkelstein A, Shima DT. A2E induces IL-1β production in retinal pigment epithelial cells via the NLRP3 inflammasome. *PLoS One*. 2013;8:e67263.
37. Sparrow JR, Parish CA, Hashimoto M, Nakanishi K. A2E, a lipofuscin fluorophore, in human retinal pigmented epithelial cells in culture. *Invest Ophthalmol Vis Sci*. 1999;40:2988–2995.
38. Allikmets R, Singh N, Sun H, et al. A photoreceptor cell-specific ATP-binding transporter gene (ABCR) is mutated in recessive Stargardt macular dystrophy. *Nat Genet*. 1997;15:236–246.
39. Jang YP, Matsuda H, Itagaki Y, Nakanishi K, Sparrow JR. Characterization of peroxy-A2E and furan-A2E photooxidation products and detection in human and mouse retinal pigment epithelial cell lipofuscin. *J Biol Chem*. 2005;280:39732–39739.
40. Wu Y, Yanase E, Feng X, Siegel M, Sparrow J. Structural characterization of bisretinoid A2E photocleavage products and implications for age-related macular degeneration. *Proc Natl Acad Sci U S A*. 2010;107:7275–7280.
41. Kim S, Jang Y, Jockusch S, Fishkin NE, Turro NJ, Sparrow JR. The all-*trans*-retinal dimer series of lipofuscin pigments in retinal pigment epithelial cells in a recessive Stargardt disease model. *Proc Natl Acad Sci U S A*. 2007;104:19273–19278.
42. Feeney-Burns L, Hilderbrand ES, Eldridge S. Aging human RPE: morphometric analysis of macular, equatorial, and peripheral cells. *Invest Ophthalmol Vis Sci*. 1984;25:195–200.
43. von Rückmann A, Fitzke FW, Bird AC. Fundus autofluorescence in age-related macular disease imaged with a laser scanning ophthalmoscope. *Invest Ophthalmol Vis Sci*. 1997;38:478–486.
44. Okubo A, Rosa R, Bunce CV, et al. The relationships of age changes in retinal pigment epithelium and Bruch's membrane. *Invest Ophthalmol Vis Sci*. 1999;40:443–449.
45. Delori FC, Goger DG, Dorey CK. Age-related accumulation and spatial distribution of lipofuscin in RPE of normal subjects. *Invest Ophthalmol Vis Sci*. 2001;42:1855–1866.
46. Boyer NP, Higbee D, Currin MB, et al. Lipfuscin and *N*-retinylidene-*N*-retinylethanolamine (A2E) accumulate in retinal pigment epithelium in absence of light exposure: their origin is 11-*cis*-retinal. *J Biol Chem*. 2012;287:22276–22286.
47. Sparrow JR, Vollmer HR, Zhou J, et al. A2E-epoxides damage DNA in retinal pigment epithelial cells. *J Biol Chem*. 2003;278:18207–18213.
48. Chu XK, Wang Y, Ardeljan D, Tuo J, Chan CC. Controversial view of a genetically altered mouse model of focal retinal degeneration. *Bioengineered*. 2013;4:130–135.
49. Popp N, Chu XK, Shen D, Tuo J, Chan CC. Evaluating potential therapies in a mouse model of focal retinal degeneration with age-related macular degeneration (AMD)-like lesions. *J Clin Exp Ophthalmol*. 2013;4:1000296.
50. Mehalow AK, Kameya S, Smith RS, et al. CRB1 is essential for external limiting membrane integrity and photoreceptor morphogenesis in the mammalian retina. *Hum Mol Genet*. 2003;12:2179–2189.
51. Pellissier LP, Alves CH, Quinn PM, et al. Targeted ablation of CRB1 and CRB2 in retinal progenitor cells mimics Leber congenital amaurosis. *PLoS Genet*. 2013;9:e1003976.
52. Allan LA, Clarke PR. Phosphorylation of caspase-9 by CDK1/cyclin B1 protects mitotic cells against apoptosis. *Mol Cell*. 2007;26:301–310.
53. Li J, Zhang Y, Cai X, et al. All-*trans*-retinal dimer formation alleviates the cytotoxicity of all-*trans*-retinal in human retinal pigment epithelial cells. *Toxicology*. 2016;371:41–48.

Investigative Ophthalmology & Visual Science